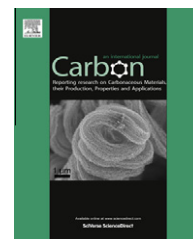


Available at www.sciencedirect.com

SciVerse ScienceDirect

journal homepage: www.elsevier.com/locate/carbon

A graphene-based large area surface-conduction electron emission display

Wei Lei ^{a,*}, Chi Li ^{a,b}, Matthew T. Cole ^b, Ke Qu ^a, Shuyi Ding ^a, Yan Zhang ^b,
 Jamie H. Warner ^c, Xiaobing Zhang ^a, Baoping Wang ^a, William I. Milne ^{b,d}

^a Display Research Centre, School of Electronic Science and Engineering, Southeast University, Nanjing 210096, PR China

^b Department of Engineering, Electrical Engineering Division, University of Cambridge, 9 JJ Thomson Avenue, CB3 0FA Cambridge, United Kingdom

^c Department of Materials, University of Oxford, Parks Road, Oxford OX1 3PH, United Kingdom

^d Department of Information Display, Kyung Hee University, Seoul 130-701, Republic of Korea

ARTICLE INFO

Article history:

Received 18 October 2012

Accepted 6 January 2013

Available online 16 January 2013

ABSTRACT

The fabrication and functionality of a 21 cm graphene-based transverse electron emission display panel is presented. A screen-printed triode edge electron emission geometry has been developed based on chemical vapor deposited (CVD) graphene supported on vertically aligned carbon nanotubes (CNT) necessary to minimize electrostatic shielding induced by the proximal bulk substrate. Integrated ZnO tetrapod electron scatterers have been shown to increase the emission efficiency by more than 90%. Simulated electron trajectories validate the observed emission characteristics with driving voltages less than 60 V. Fabricated display panels have shown real-time video capabilities that are hysteresis free (<0.2%), have extremely stable lifetimes (<3% variation over 10 h continuous operation) in addition to rapid temporal responses (<1 ms).

© 2013 Elsevier Ltd. All rights reserved.

1. Introduction

The outstanding electrical [1], mechanical [2,3], and chemical [4,5] properties of low-dimensional nanocarbons, in particular graphene and carbon nanotubes (CNT), make them attractive materials for next-generation transparent electrodes in state-of-the-art display technologies [6–8]. Graphene and CNTs have simultaneously high electrical and optical conductivities with near-zero band gaps [9–11]. The atomic thickness of graphene endows it with an exceptionally high aspect ratio, potentially higher even than CNTs, whilst defective edge terminations rich in dangling bonds render graphene superior to CNTs for highly efficient electron tunneling [12], both of which qualifies graphene as a striking candidate for a variety of field emission applications.

Linear dispersion in graphene gives rise to consequent massless fermions and in the presence of an electric field this allows field emission liberated electrons to avoid all backscattering as their escape velocity is independent of their energy. As such, graphene and many other graphitic nanocarbons are some of the best field emitting electron sources available to date. Recently many reports on field emission from graphene have emerged [7,8,12–14]. Pristine exfoliated graphene sheets have shown turn-on electric fields as low as $0.1 \text{ V } \mu\text{m}^{-1}$ [12,15–17]. Homogeneous, single-layer graphene deposited by electrophoresis has similarly demonstrated excellent field-emission properties such as turn on electric fields from $2.3 \text{ V } \mu\text{m}^{-1}$ and field enhancement factors of up to 3700 [12,13]. Threshold fields of $\sim 1.5 \text{ V } \mu\text{m}^{-1}$ with field enhancement factors in excess of 4500 have also been reported from screen printed graphene films [7]. Graphene field emitting

* Corresponding author.

E-mail address: lw@seu.edu.cn (W. Lei).

0008-6223/\$ - see front matter © 2013 Elsevier Ltd. All rights reserved.

<http://dx.doi.org/10.1016/j.carbon.2013.01.004>

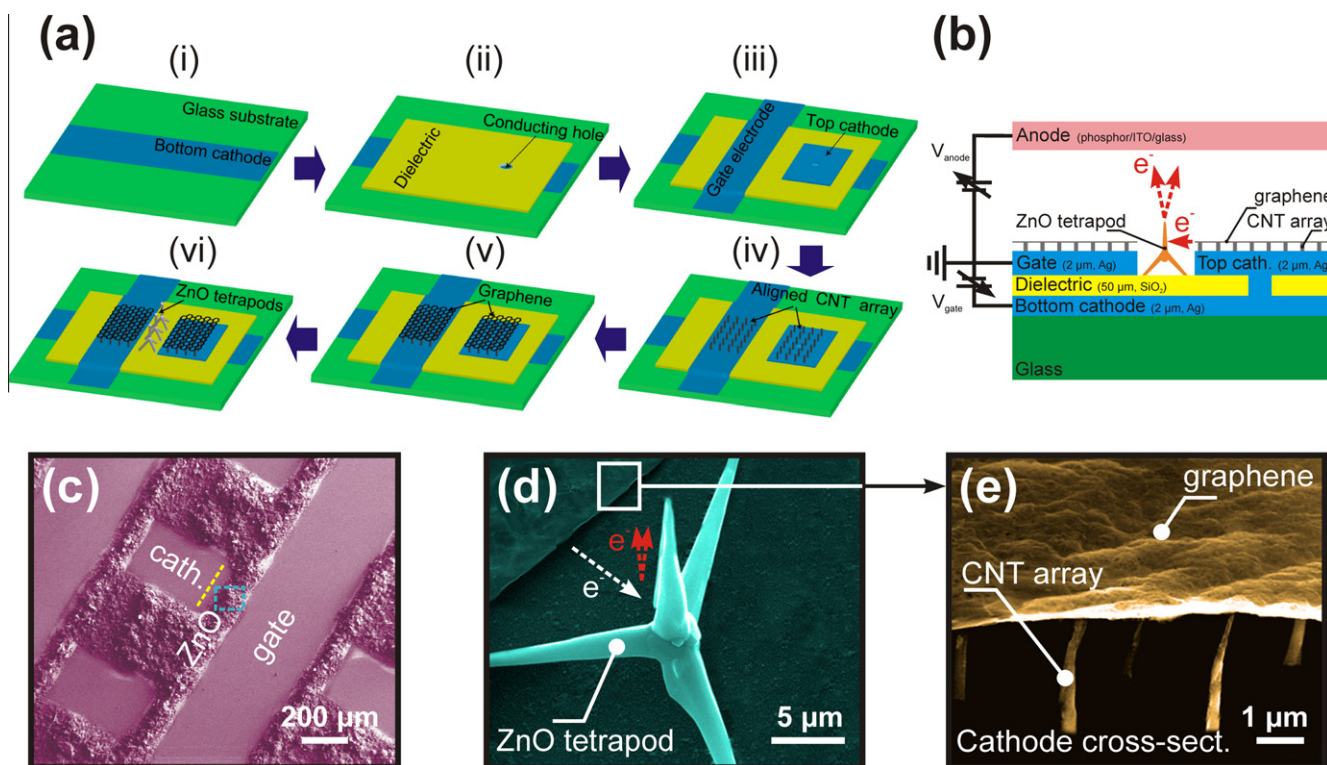


Fig. 1 – (a) Fabrication of the graphene edge field emission structure; (i) Screen printed Ag (2 μm) bottom cathode on a glass substrate (3 mm). (ii) Screen printed 50 μm SiO₂ dielectric and subsequent buffered hydro fluoric acid wet etching for via formation. (iii) Screen printed Ag (2 μm) gate and top cathode. (iv) Chemical vapor deposition of Ni catalyzed vertically aligned carbon nanotubes directly onto the gate and cathode. (v) Graphene transferred onto the CNT arrays. (vi) Screen-printing of the ZnO tetrapod electron scatterers between the gate and top cathode. (b) Cross-section schematic of the display. The electrodes forming the triode structure are the Ag gate, the Ag top cathode and the phosphor/ITO/glass anode which are separated from the glass gate-cathode substrate by 3 mm ceramic spacers. (c) A scanning electron micrograph (false colored) of a complete graphene edge emission structure showing the gate and cathode (cath.) electrodes, as well as the ZnO tetrapod electron scatterers (Scale bar: 200 μm). (d) A scanning electron micrograph (false colored) of a single ZnO tetrapod and graphene edge (Scale bar: 5 μm). (e) A cross-section scanning electron micrograph (false colored) of the cathode, as indicated by the dashed line in (c), showing the graphene edge emitter supported by an array of CNT bundles (Scale bar: 1 μm). Note that the cross-section of the gate electrode has an equivalent structure.

arrays on Cu foil, fabricated by conventional photolithography and wet etching techniques, offer one possible route to micron-scale planar emitters over large areas, though such structures offer relatively poor turn-on fields ($\sim 7.2 \text{ V } \mu\text{m}^{-1}$ [8]). Impressive emission stability and uniformity, significantly better than graphene-powders and comparable to CNTs, have also been demonstrated [12]. Nevertheless, such solution-based graphene deposition results in flakes that are oriented at various uncontrolled and irreproducible angles relative to the substrate, making such approaches largely non-scalable.

Though the lateral size to thickness ratio of graphene is exceptionally large, in order to fully exploit this field enhancement in traditional vertical emitter geometries the graphene must stand on edge rather than lay in-plane on the substrate, as such morphologies offer comparatively poor emission performance [18]. However, obtaining vertically aligned graphene sheets is currently challenging. Microwave plasma chemical vapor deposition has been used elsewhere to synthesize promising carbon nanowall field emitters [19,20]. Nevertheless, almost all reports on

in situ and *ex situ* graphene growth, exfoliation, and deposition techniques have thus far yielded flat sheets lying adjacent to, and in intimate contact with their substrate. Although an improvement in field emission performance has certainly been observed [13] – a consequence of lattice defects and free edge-bond formation induced by chemical and thermal post treatments – such emitters are difficult to integrate into practical displays due to their poor topographic uniformity and emission reproducibility. Exploiting the lateral, in-plane emission properties of graphene is perhaps the most scalable route to the eventual integration of graphene into field emission systems, especially following the recent advancements in ultra-large-area CVD graphene single crystal growth [21]. Despite this, to fully realise the maximum field enhancement the graphene edge emitters must be supported above the proximal bulk substrate to ensure negligible substrate-induced electrostatic shielding [22]. Herein, we report a new graphene-based transverse field emission structure employing graphene edge emitters supported on arrays of CNTs with integrated electron scattering ZnO tetrapods.

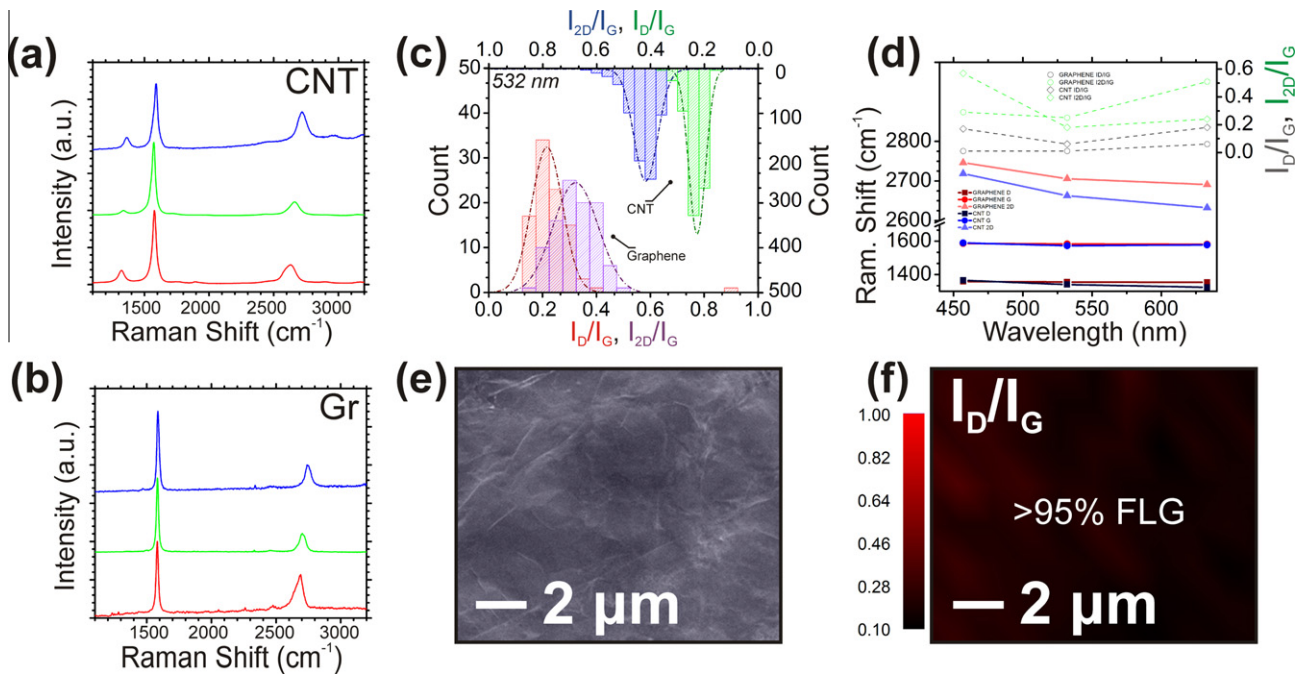


Fig. 2 – Graphene and CNTs by thermal chemical vapor deposition. Raman spectra (at 457 nm (blue), 532 nm (green) and 633 nm (red) excitation) of; (a) CNTs and (b) graphene (Gr). (c) I_D/I_G and I_{2D}/I_G distributions for the graphene edge emitter and CNT supports (532 nm excitation). (d) Graphene and CNT dispersion relation for I_D/I_G (grey), I_{2D}/I_G (green) and Raman shift of the D (■), G (●) and 2D (▲) peaks. (e) A scanning electron micrograph of a graphene film (Scale bar: 2 μm) and (f) the corresponding I_D/I_G map (Scale bar: 2 μm), both highlighting the uniformity of the graphene. More than 95% of the graphene is few layer graphene (FLG), as determined from I_{2D}/I_G data (not shown). (For interpretation of the references to color in this figure legend, the reader is referred to the web version of this article.)

The graphene edge electron emitter is a planar triode where the cathode and gate electrodes align orthogonally. To passivate the substrate induced electric field shielding [23] CNT arrays (1.5 μm height/0.2 μm bundle diameter/2 μm pitch) were employed to mechanically elevate and electrically connect to the graphene electron emitter (Fig. 2b). The emission performance was dramatically enhanced by employing secondary and back-scattered electron sites formed from ZnO. ZnO was selected as it has a high secondary electron yield of 2.3 [24], has a wide variety of morphologies that are solution processable, and can be synthesized inexpensively at low temperatures. ZnO nanowires and nanorods showed inferior performance compared to ZnO tetrapods. The one dimensional ZnO nanowires and nanorods were more compact and tended to aggregate more readily resulting in denser films with significantly less scattering capabilities. Moreover, the nanowires and nanorods often aligned parallel to the substrate and the field enhancement associated with their geometry was not fully realized. In contrast the morphology of the tetrapods ensured that at least a single axis offered zones of high field enhancement.

2. Experimental

2.1. Display fabrication

The fabrication process of the edge emission triode is detailed in Fig. 1a. Glass substrates were screen printed with a bottom

cathode (Ag, 2 μm), an SiO_2 dielectric layer, top cathode (Ag, 2 μm), and gate electrode (Ag, 2 μm). The 50 μm screen printed SiO_2 dielectric suspension separates the cathode and gate. Arrays of vias were etched in the dielectric using buffered hydrofluoric acid such that the cathode is in plane with the gate electrode. The cathode and gate were subsequently magnetron sputtered with Ni dots to catalyze CNT growth, as described below. Panels were then coated with graphene supported on an SU-8 mediator. The edge electron emitter was then patterned by photolithography directly on the graphene/SU-8. Finally, graphene was patterned by oxygen reactive ion etching (20 W, 30 s). A typical completed device is shown in Fig. 1c.

2.1.1. CNT, graphene, and ZnO tetrapod synthesis

2.1.1.1. Carbon nanotubes. CNTs were grown from d.c. magnetron sputtered Ni catalysts (15 nm, 99.99%, Beijing Zhongjingkeyi Technology Co., Ltd.) on Ag-coated glass cathodes patterned using conventional photolithography. Vertically aligned multi-walled CNT bundles were synthesized by thermal chemical vapor deposition (CVD) in a commercially available cold-wall reactor (Black Magic, Aixtron Ltd.). Catalyst samples were annealed in Ar (Grade 4.0) at 420 $^\circ\text{C}$ (5 $^\circ\text{C s}^{-1}$) for 40 s with subsequent exposure to C_2H_2 (200 sccm, Grade 4.0) in a NH_3 ballast (50 sccm, Grade 4.0) at 450 $^\circ\text{C}$ and 1.4×10^3 Pa. Following a 60 s growth the multi-walled CNTs were 10.0 ± 0.6 (± 1 S.D.) μm in length and 50 ± 2 (± 1 S.D.) nm in diameter.

2.1.1.2. Graphene. Graphene was synthesized in a custom-built thermal CVD tube furnace. Cu catalysts (foil, 99.99%, Beijing Zhongjingkeyi Technology Co., Ltd.) were heated to 1000 °C (4 °C s^{-1}) and exposed to CH_4 (40 sccm, Grade 4.0) and H_2 (40 sccm, Grade 4.0) at 100 Pa. Pristine graphene was transferred to the supporting CNT arrays (cathode) using an SU-8 (2000, MicroChem Corp.) mediator and wet-etching of the underlying Cu (aqueous FeCl_3 (25 wt.%), Nanjing Chemical Solution Corp.) [25,26]. SU-8 was removed by dissolution in acetone.

2.1.1.3. ZnO tetrapods. ZnO tetrapods were synthesized by non-catalytic vapor phase transport of Ar (200 sccm, Grade 4.0) and O_2 (100 sccm, Grade 4.0) at 10^4 Pa in a custom-built horizontal tube furnace operated at 900 °C (4 °C s^{-1}). The ZnO tetrapods were collected and mixed with ethyl cellulose ethoce terpeneol. A $10\text{ }\mu\text{m}$ thick film was subsequently screen-printed (NewLong Seimitsu) between the cathode and gate using this paste.

2.2. Materials characterization

2.2.1. CNTs and graphene

Fig. 2a and b show the Raman spectra of the CNTs and graphene, respectively, acquired at 457 nm (blue), 532 nm (green), and 633 nm (red) excitations. Fig. 2e and f show a scanning electron micrograph and the corresponding Raman intensity ratio of the D and G peaks (I_D/I_G) spatially resolved (532 nm), highlighting the uniformity of the CVD-deposited graphene. The graphene is >95% few layer graphene with an $I_D/I_G = 0.21 \pm 0.09$ and $I_{2D}/I_G = 0.30 \pm 0.07$ (± 1 S.D.) (Fig. 2b) [27]. The asymmetric fourfold Lorentzian-fitted 2D peak (2704 cm^{-1}) of the graphene has a full-width half-maximum of $\sim 51.8\text{ cm}^{-1}$, suggesting the presence of highly graphitic turbostratic strata [28,29]. The CNTs are multi-walled and have an $I_D/I_G = 0.21 \pm 0.03$ and $I_{2D}/I_G = 0.41 \pm 0.05$ (± 1 S.D.) (Fig. 2b and c). The CNTs (and graphene) have D, G and 2D peak dispersions of 0.235 (0.026) $\text{cm}^{-1}\text{ nm}^{-1}$, 0.062 (0.025) $\text{cm}^{-1}\text{ nm}^{-1}$, and 0.480 (0.305) $\text{cm}^{-1}\text{ nm}^{-1}$ (Fig. 2d), respectively, consistent with high quality graphitic CVD nanocarbons [29].

2.2.2. ZnO tetrapods

Fig. 3a shows an X-ray diffraction (XRD) pattern from the as-synthesized ZnO tetrapods [30]. All diffraction peaks are attributed to the ZnO hexagonal wurtzite crystal with lattice constants of $a = 3.249\text{ \AA}$ and $c = 5.205\text{ \AA}$ – consistent with JCPDS card No. 89-0511. High-resolution transmission electron microscopy and select-area electron diffractograms (Insets, Fig. 3a) confirm this, with a measured lattice constant of $0.32 \pm 0.03\text{ nm}$ and an approximate d -spacing of 0.28 nm . No impurity diffraction peaks were detected. Energy dispersive X-ray spectroscopy corroborates this (Fig. 3b), evidencing a Zn-rich O:Zn ratio of 1:3.47 [31]. The Tauc gap was estimated to be 3.68 eV , further evidencing the high quality of the as-synthesized ZnO tetrapods (Fig. 3c) [32].

2.2.3. Techniques

CNTs and graphene were analyzed using a polychromatic Raman spectrometer (Renishaw InVia) fitted with fused-silica optics and a piezo stage (nominal step size = $0.2\text{ }\mu\text{m}$) with a

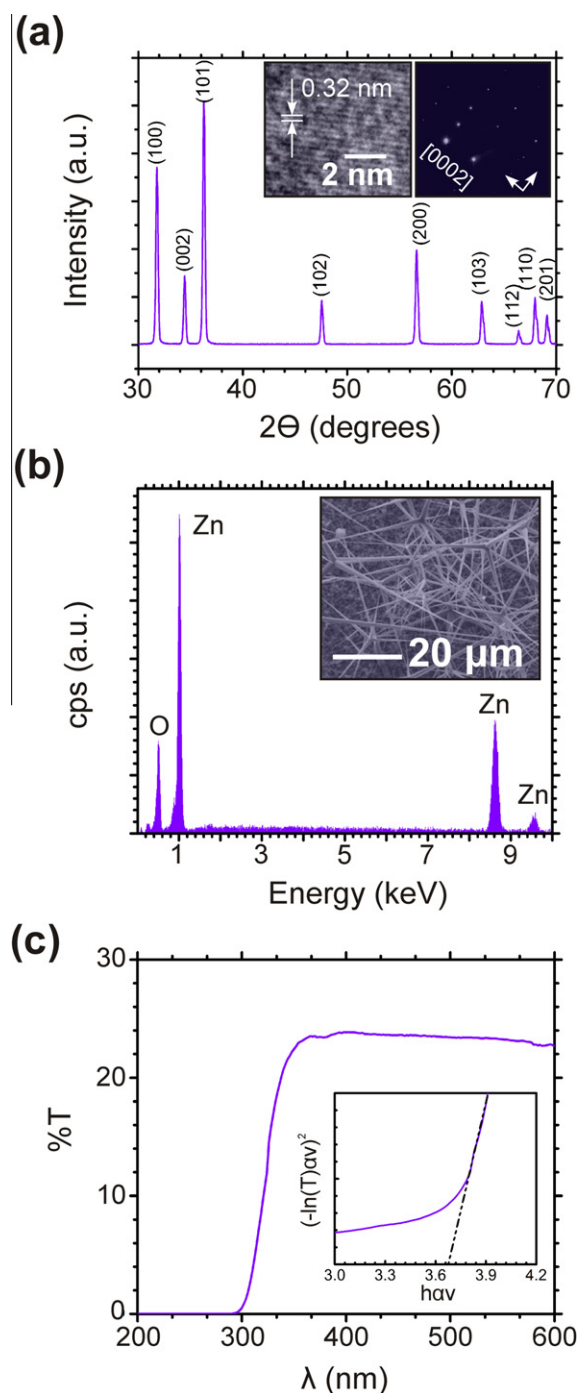


Fig. 3 – ZnO tetrapod electron scatterers synthesized by non-catalytic vapor phase transport. (a) X-ray diffraction pattern of the as-synthesized ZnO tetrapods. Inset: High-resolution electron micrograph and the corresponding select area diffraction pattern showing the regular wurtzite crystal structure (Scale bar: 2 nm) with a lattice constant of $0.32 \pm 0.03\text{ nm}$. (b) Energy dispersive X-ray spectrum highlighting the stoichiometry of the synthesized ZnO tetrapods. Inset: Scanning electron micrograph of as-synthesized ZnO tetrapods (Scale bar: $20\text{ }\mu\text{m}$). (c) UV-Vis spectrum showing a Tauc gap of 3.68 eV .

probe diameter of $1.2\text{ }\mu\text{m}$ and a $100\times$ aperture. Excitation sources at 457, 532, and 633 nm with incident powers

<10 mW were used throughout. Triplicate accumulations and a 20 s integration time were used to optimize the signal-to-noise. Scanning electron micrographs were acquired using a Quanta 20 FEI and a variable pressure Carl Zeiss Gemini-Sigma scanning electron microscopes operated at 1 kV. An aberration corrected FEI Titan³ 80–300 in scanning mode with bright-field and annular dark-field detectors, and a JEOL JEM-4000 EX high-resolution transmission electron microscope were employed to image the crystalline structure of the ZnO tetrapods and to record the corresponding select area diffraction patterns. X-ray diffraction measurements were performed using an ARL X'TRA powder diffractometer (Thermo Scientific) with an integrated Peltier cooled Si(Li) solid state detector and a low-angle resolution down to 0.5°. A UV-Vis (deuterium/tungsten) spectrophotometer (Thermo Scientific), with a 2 nm spectral resolution and a beam size of 1 cm², was used for Tauc gap measurements.

2.3. Field emission measurements

Field emission measurements were performed using a custom-built turbo-molecular pumped chamber evacuated to $<10^{-4}$ Pa attached to computer controlled source-measure

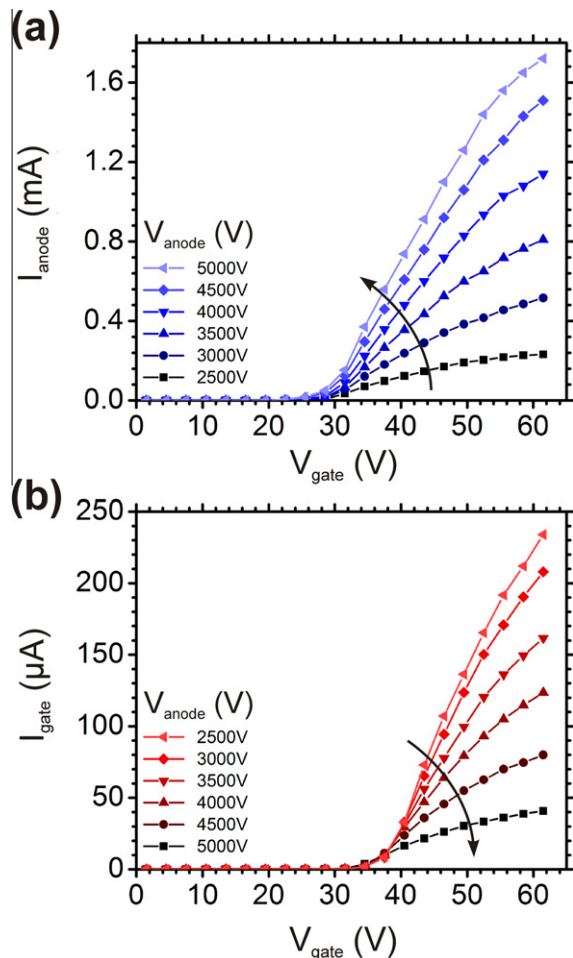


Fig. 4 – Electron emission performance. (a) Anode current (I_{anode}) and (b) gate current (I_{gate}) as a function of gate voltage (V_{gate}) and anode voltage (V_{anode}).

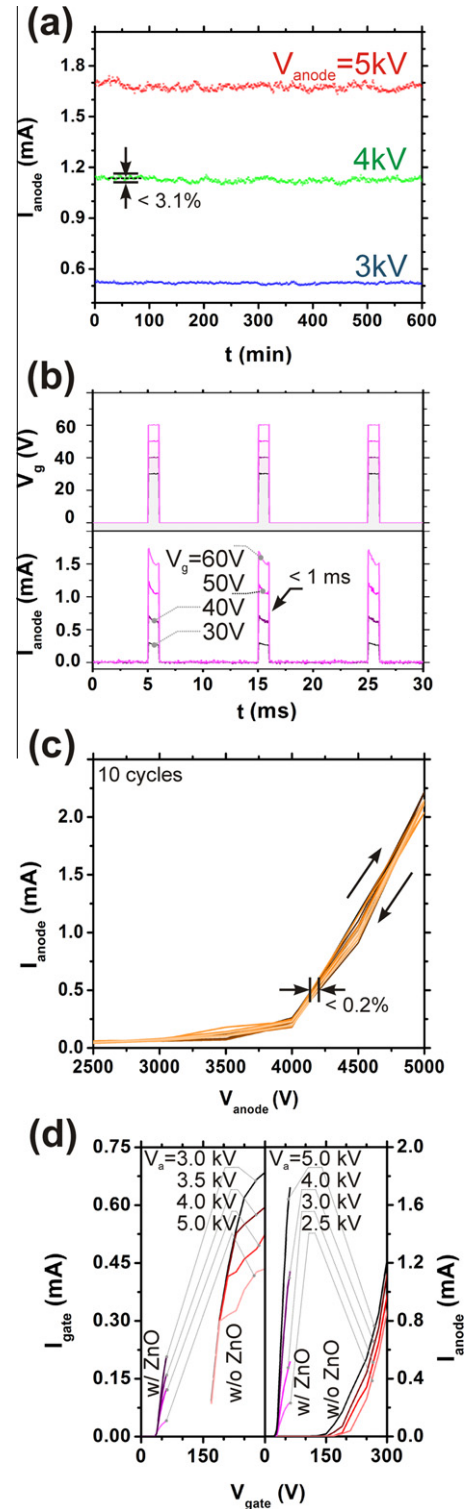


Fig. 5 – (a) Room temperature accelerated lifetime measurement performed at 10^{-5} Pa ($V_{\text{anode}} = 3, 4, 5$ kV, $V_{\text{gate}} = 60$ V) showing minor variations in I_{anode} of $\pm 3.18\%$, $\pm 3.08\%$ and $\pm 2.92\%$, respectively. (b) Pulsed gate response ($V_{\text{gate}} = 30, 40, 50, 60$ V, $V_{\text{anode}} = 5$ kV) showing an on/off time of < 1 ms. (c) I_{anode} hysteresis performance over 10 cycles ($V_{\text{gate}} = 60$ V), showing negligible up-shift ($< 0.2\%$ at $I_{\text{anode}} = 0.5$ mA). (d) Electron emission with (w/) and without (w/o) the ZnO tetrapod electron scatters. The ZnO tetrapods are seen to increase the I_{anode} by 39.8%.

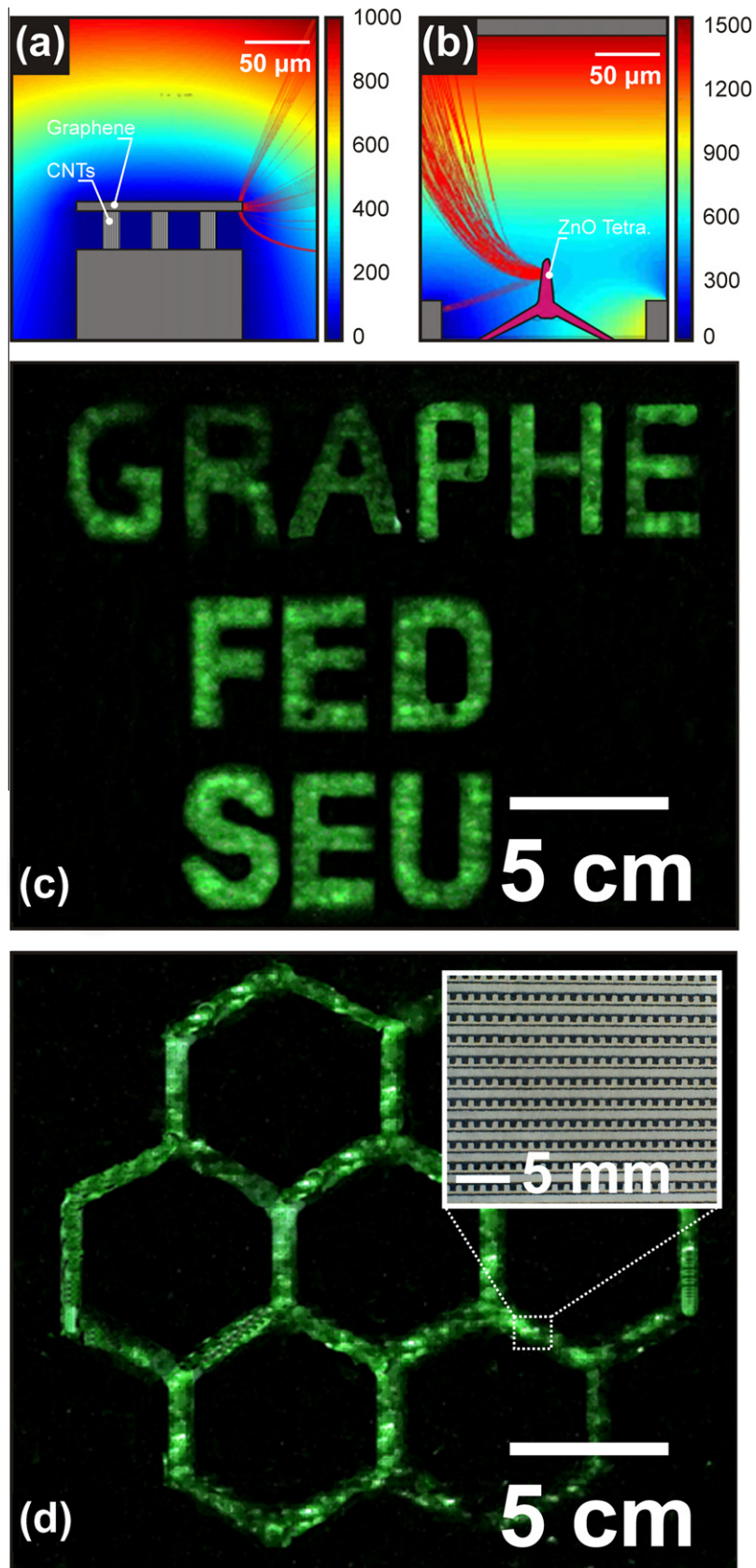


Fig. 6 – (a) Simulated potential distribution (color bar, V) and electron trajectories (red curves) at the graphene edge, and (b) the ZnO tetrapod electron scatter site. (c and d) Optical micrographs of a prototype 21 cm diagonal graphene electron emission display. Inset: Optical micrograph of a 23 pixel × 11 pixel section of a fabricated display panel. (For interpretation of the references to colour in this figure legend, the reader is referred to the web version of this article.)

units (Keithley 6517A) and a high voltage supply. Samples were vacuum annealed at 500 °C for 24 h at 10^{-5} Pa prior to loading into the field emission testing system where samples were further baked at 180 °C for 24 h to ensure complete removal of surface absorbates and residual organics.

3. Results and discussion

The dependencies of the anode current (I_{anode}) and gate current (I_{gate}) on the gate voltage (V_{gate}) are shown in Fig. 4a and b. I_{anode} is strongly dependent on the V_{gate} . For $V_{\text{gate}} < 30$ V few electrons were emitted from the graphene edges. However, I_{anode} is strongly influenced by the anode voltage (V_{anode}). If the electric field between cathode and anode is much less than the electric field established between the cathode and gate any secondary emitted electrons (SEEs) and back-scattered electrons (BSEs) yielded from the ZnO tetrapods will be attracted toward the gate electrode. This gives rise to an unsatisfactorily large I_{gate} . Thus, I_{anode} reduces. For a fixed V_{anode} , both I_{anode} and I_{gate} increase with increasing V_{gate} , with a saturating response at about 60 V (Fig. 4). However, whilst I_{anode} increases, I_{gate} decreases with increasing V_{anode} . This is primarily due to an increasing number of electrons being diverted from the gate trajectory toward the anode. The emission efficiency is therefore greater at higher anode potentials, with the highest efficiency occurring when $30 \text{ V} < V_{\text{gate}} < 60 \text{ V}$. The graphene edge emitter offers a maximum efficiency of nearly 90% with $I_{\text{anode}} = 1.2 \text{ mA}$, for $V_{\text{anode}} = 5 \text{ kV}$ and $V_{\text{gate}} = 60 \text{ V}$.

Fig. 5a shows typical room temperature accelerated lifetimes measurements ($V_{\text{gate}} = 60 \text{ V}$) performed at 10^{-5} Pa. The emission is highly stable with variations in anode currents of only $\pm 3.18\%$ ($V_{\text{anode}} = 3 \text{ kV}$), $\pm 3.08\%$ (4 kV), and $\pm 2.92\%$ (5 kV), which also demonstrates the near-zero burn-in/conditioning time of the emitters. ZnO tetrapod films were electrically continuous and were connected to the gate electrode. There was negligible charge build-up during emission. Indeed, the negligible drift during the emission current lifetime test confirms this. If charging were to occur it would undoubtedly manifest as a weakly parabolic shift over time in the emission current. However, the emission during the stability tests was stochastic, thereby supporting the notion of negligible charging effects.

Fig. 5b depicts the emission behavior of the anode current in response to pulsed gate voltages ($V_{\text{gate}} = 30, 40, 50, 60 \text{ V}$). Extremely fast on times of $< 1 \text{ ms}$ were noted under all gate conditions. The hysteresis performance of the graphene edge-emitter is shown in Fig. 5c. Over 10 cycles extremely minor shifts to higher threshold extraction voltages was observed ($\Delta V_{\text{anode}}(I_{\text{anode}} = 0.5 \text{ mA}) < 0.2\%$), significantly less than other nanocarbon-based field emission sources [33,34].

The distribution of the electric potential and electron trajectories were simulated in the COMSOL Multiphysics (V. 3.3A) environment, as illustrated in Fig. 6a and b, respectively. Potential distributions were calculated using a finite difference approach. Electron trajectories (red curves) were estimated using the Forth Runge Kutta formalism.

ZnO is an *n*-type wide band-gap semiconductor. When electrons bombard the ZnO tetrapods SEEs are liberated, as are BSEs generated by the reflected impinging electrons. The

initial energy of the field emitted electrons is low and linearly scales with anode bias [35]. The electric field surrounding the emitters is particularly intense ($5 \text{ V } \mu\text{m}^{-1}$). When a bias is applied to the gate electrode a strong electric field is established at the graphene edge, attributed to its high in-plane aspect ratio. The CNT array decouples the graphene edge-emitter from the substrate thereby enhancing the fringe field. As Fig. 6b shows, these primary electrons are accelerated by the electric field established between the cathode and gate. The electrons then bombard the ZnO tetrapods and increase the emission current substantially whilst also reducing the gate voltage necessary to extract a given current density. SEEs and BSEs give rise to the increased I_{anode} , as $I_{\text{anode}} = I_{\text{Gr}} + I_{\text{SEE}}$, where I_{Gr} is the current associated with the electrons liberated from the graphene edge and I_{SEE} is the additional current associated with the ZnO tetrapod secondary electron emission. Graphitic nanocarbons, and graphene in particular have extremely low secondary electron and back-scattered electron yields [36]. Thus, all SEEs can be attributed exclusively to the ZnO tetrapods. This increase in the available electron population is clearly evidenced in Fig. 5d where the emission current with and without the ZnO tetrapods is shown. Integration of the ZnO tetrapods reduces the gate current by a factor of two. In the absence of the ZnO tetrapods approximately 36% of the emission current leaks to the gate, whereas integration of the ZnO tetrapod electron scatter sites results in a dramatic reduction to 2.4% under equivalent extraction conditions ($V_{\text{anode}} = 5 \text{ kV}$). ZnO tetrapods increase the anode current by 39.8% ($V_{\text{anode}} = 5 \text{ kV}$) under a gate voltage approximately five times smaller than in emitters without the ZnO tetrapods.

A fully sealed 320×240 pixel (21 cm diagonal) graphene-based electron emission display panel has been fabricated based on the reported graphene edge emitter geometry. The display panel employs a ZnO: Zn phosphor and is operated at 5×10^{-5} Pa, $V_{\text{g}} = 60 \text{ V}$ and $V_{\text{anode}} = 5 \text{ kV}$. Individual pixel addressing and real-time video rate movies have been demonstrated (see Supplementary Information). Fig. 6c and d show typical optical images of the display panel indicating the high degree of uniformity afforded.

4. Conclusions

Here we report on the fabrication and functionality of a large-area CNT-supported graphene triode electron edge emission display employing electron scattering ZnO tetrapods. Simulated edge electron trajectories validated the measured emission characteristics. Low driving voltages ($< 60 \text{ V}$) with high emission efficiency ($> 90\%$) were obtained. Low hysteresis ($< 0.2\%$), extremely stable lifetimes ($< 3\%$ variation over 10 h) and fast ($< 1 \text{ ms}$) emission characteristics have been observed. A monochromatic 21 cm diagonal display, based on a graphene edge electron emitter, capable of real-time video has been demonstrated for the first time.

Acknowledgements

This work is supported by National Key Basic Research Program 973 (2010CB327705), National Natural Science

Foundation Project (51120125001, 51202027, 51002031, 61101023), China Postdoctoral Science Foundation (2012M511648), Foundation of Doctoral Program of Ministry of Education (20100092110015), and the Research Fund for International Young Scientists from NSFC (51050110142). The Authors' thank the Cavendish Laboratory, Cambridge University for the kind use of their Raman facilities. M.T.C acknowledges St Edmund's College Cambridge University and the Isaac Newton Trust, Trinity College Cambridge University, for generous financial support.

Appendix A. Supplementary data

Supplementary data associated with this article can be found, in the online version, at <http://dx.doi.org/10.1016/j.carbon.2013.01.004>.

REFERENCES

- Geim AK, Novoselov KS. The rise of graphene. *Nat Mater* 2007;6(3):183–91.
- Lee C, Wei X, Kysar JW, Hone J. Measurement of the elastic properties and intrinsic strength of monolayer graphene. *Science* 2008;321(5887):385–8.
- Bunch JS, Verbridge SS, Alden JS, van der Zande AM, Parpia JM, Craighead HG, et al. Impermeable atomic membranes from graphene sheets. *Nano Lett* 2008;8(8):2458–62.
- Elias DC, Nair RR, Mohiuddin TMG, Morozov SV, Blake P, Halsall MP, et al. Control of graphene's properties by reversible hydrogenation: evidence for graphane. *Science* 2009;323(5914):610–3.
- Wang X, Li X, Zhang L, Yoon Y, Weber PK, Wang H, et al. N-doping of graphene through electrothermal reactions with ammonia. *Science* 2009;324(5928):768–71.
- Bae S, Kim H, Lee Y, Xu XF, Park JS, Zheng Y, et al. Roll-to-roll production of 30-inch graphene films for transparent electrodes. *Nat Nanotechnol* 2010;5(8):574–8.
- Qian M, Feng T, Ding H, Lin L, Li H, Chen Y, et al. Electron field emission from screen-printed graphene films. *Nanotechnology* 2009;20(42):425702.
- Huang C-K, Ou Y, Bie Y, Zhao Q, Yu D. Well-aligned graphene arrays for field emission displays. *Appl Phys Lett* 2011;98(26):263104.
- Eda G, Fanchini G, Chhowalla M. Large-area ultrathin films of reduced graphene oxide as a transparent and flexible electronic material. *Nat Nanotechnol* 2008;3(5):270–4.
- Tombros N, Jozsa C, Popinciuc M, Jonkman HT, van Wees BJ. Electronic spin transport and spin precession in single graphene layers at room temperature. *Nature* 2007;448(7153):571–4.
- Novoselov KS, Geim AK, Morozov SV, Jiang D, Zhang Y, Dubonos SV, et al. Electric field effect in atomically thin carbon films. *Science* 2004;306(5696):666–9.
- Wu Z-S, Pei S, Ren W, Tang D, Gao L, Liu B, et al. Field emission of single-layer graphene films prepared by electrophoretic deposition. *Adv Mater* 2009;21(17):1756–60.
- Dong J, Zeng B, Lan Y, Tian S, Shan Y, Liu X, et al. Field emission from few-layer graphene nanosheets produced by liquid phase exfoliation of graphite. *J Nanosci Nanotechnol* 2010;10(8):5051–5.
- Tsai JTH, Chu TYE, Shiu J-Y, Yang C-S. Field emission from an individual freestanding graphene edge. *Small* 2012;8(24):3739–45.
- Lee SW, Lee SS, Yang E-H. A Study on field emission characteristics of planar graphene layers obtained from a highly oriented pyrolyzed graphite block. *Nano Res Lett* 2009;4(10):1218–21.
- Wang HM, Zheng Z, Wang YY, Qiu JJ, Guo ZB, Shen ZX, et al. Fabrication of graphene nanogap with crystallographically matching edges and its electron emission properties. *Appl Phys Lett* 2010;96(2):023106.
- Yamaguchi H, Murakami K, Eda G, Fujita T, Guan P, Wang W, et al. Field emission from atomically thin edges of reduced graphene oxide. *ACS Nano* 2011;5(6):4945–52.
- Xiao Z, She J, Deng S, Tang Z, Li Z, Lu J, et al. Field electron emission characteristics and physical mechanism of individual single-layer graphene. *ACS Nano* 2010;4(11):6332–6.
- Zhang Y, Du J, Tang S, Liu P, Deng S, Chen J, et al. Optimize the field emission character of a vertical few-layer graphene sheet by manipulating the morphology. *Nanotechnology* 2012;23(1):015202.
- Wu Yang. Effects of localized electric field on the growth of carbon nanowalls. *Nano Lett* 2002;2(4):355–9.
- Yan Z, Lin J, Peng Z, Sun Z, Zhu Y, Li L, et al. Toward the synthesis of wafer-scale single-crystal graphene on copper foils. *ACS Nano* 2012;6(10):9110–7.
- Nilsson L, Groening O, Emmenegger C, Kuettel O, Schaller E, Schlapbach L, et al. Scanning field emission from patterned carbon nanotube films. *Appl Phys Lett* 2000;76(15):2071–3.
- De Jonge N, Bonard JM. Carbon nanotube electron sources and applications. *Philos Trans R Soc A* 2004;362(1823):2239–66.
- Huang L, Lau SP, Yang HY, Yu SF. Local measurement of secondary electron emission from ZnO-coated carbon nanotubes. *Nanotechnology* 2006;17(6):1564–7.
- Reina A, Son H, Jiao L, Fan B, Dresselhaus MS, Liu Z, et al. Transferring and identification of single- and few-layer graphene on arbitrary substrates. *J Phys Chem C* 2008;112(46):17741–4.
- Reina A, Jia XT, Ho J, Nezich D, Son HB, Bulovic V, et al. Large area, few-layer graphene films on arbitrary substrates by chemical vapor deposition. *Nano Lett* 2009;9(1):30–5.
- Lucchese MM, Stavale F, Ferreira EHM, Vilani C, Moutinho MVO, Capaz RB, et al. Quantifying ion-induced defects and Raman relaxation length in graphene. *Carbon* 2010;48(5):1592–7.
- Ferrari AC. Raman spectroscopy of graphene and graphite: disorder, electron-phonon coupling, doping and nonadiabatic effects. *Solid State Commun* 2007;143(1–2):47–57.
- Ferrari AC, Meyer JC, Scardaci V, Casiraghi C, Lazzeri M, Mauri F, et al. Raman spectrum of graphene and graphene layers. *Phys Rev Lett* 2006;97(18):187401.
- Li C, Hou K, Lei W, Zhang X, Wang B, Sun XW. Efficient surface-conducted field emission from ZnO nanotetrapods. *Appl Phys Lett* 2007;91(16):163052–505.
- Tawale JS, Dey KK, Pasricha R, Sood KN, Srivastava AK. Synthesis and characterization of ZnO tetrapods for optical and antibacterial applications. *Thin Solid Films* 2010;519(3):1244–7.
- Santhaveesuk T, Wongratanaphisan D, Choopun S. Enhancement of sensor response by TiO₂ mixing and Au coating on ZnO tetrapod sensor. *Sens Actuators B Chem* 2010;147(2):502–7.
- Chen J, Li J, Yang J, Yan X, Tay B-K, Xue Q. The hysteresis phenomenon of the field emission from the graphene film. *Appl Phys Lett* 2011;99(17):173104.
- Cole MT, Hou K, Warner JH, Barnard JS, Ying K, Zhang Y, et al. In-situ deposition of sparse vertically aligned carbon

-
- nanofibres on catalytically activated stainless steel mesh for field emission applications. *Diamond Relat Mater* 2012;23:66–71.
- [35] Fransen MJ, van Rooy TL, Kruit P. Field emission energy distributions from individual multiwalled carbon nanotubes. *Appl Surf Sci* 1999;146(1–4):312–27.
- [36] Luo J, Tian P, Pan C-T, Robertson AW, Warner JH, Hill EW, et al. Ultralow secondary electron emission of graphene. *ACS Nano* 2011;5(2):1047–55.